Dual-band gain-boosted planar lens antenna using a single layer metasurface for 6G applications

Mehrab Ramzan, and Padmanava Sen

Barkhausen Institut, Dresden, Germany
Email: {mehrab.ramzan, padmanava.sen,}@barkhauseninstitut.org

***Abstract*—In this paper, a novel dual-band planar lens antenna using single layer metasurface is proposed. The significance and fabrication feasibility of a planar lens, based on resonant structures over non-resonant structures are highlighted. The single-layer metasurface consists of multiple circular metal patches integrated with rectangular slots, aligned perpendicularly to the polarization of the antenna. The planar lens can experimentally shape and increase the gain of a single patch antenna from 7.2 dBi to 16 dBi at 10 GHz and 12.8 dBi at 10.4 GHz in the regime of X-band, eliminating the need of an array feeding network and corresponding feed losses to achieve such high antenna gains. The measurement results are in good agreement with the EM simulation results.**

I. Introduction

Convergent communication and sensing systems connecting billions of context-aware devices prove to be main focus of the future 6G wireless communication systems application platform [1]. Antenna is the key element in the radar sensing, communication and integrated systems responsible for transmitting and receiving electromagnetic waves. There is rising demand to find novel, simple and realizable ways for increasing the gain of the antenna with the increasing operating frequencies, in order to compensate for the free space path losses and to improve related sensing applications. The traditional ways of enhancing the gain by using an array of antennas suffer from complex feeding network losses apart from the substrate losses specially at cm/mmWave frequencies as the loss increases with increasing frequencies [2] [3]. X-band (8 to 12 GHz) is considered as the frequency band to validate the antenna concept. X-band is a crucial frequency range in radar and satellite communications targeting applications related to weather monitoring, air traffic, speed detection and future autonomous vehicles.

Metamaterials are promising candidates that can be used to develop very high gain antennas, miniaturized antennas, electromagnetic bandgap structures, and high impedance surfaces at different frequency ranges [4] [5] [6] [7] [8]. The simplest planar lens antenna can be designed by using a high permittivity planar superstrate with a specific thickness at a distance of $\lambda/2$ on the top of the antenna. Nevertheless, the constraint of high permittivity material with a specific thickness makes it impractical in reality [9] [10]. At the same time, metasurfaces with resonant structures have prominent features to make the fabrication of planar lens antennas possible on standard low permittivity substrate materials. The metallic unit-cell building blocks of the metasurface give extra flexibility of controlling the magnitude and phase of the signal reflected from the metasurface in order to achieve constructive interference in the far-field. In the literature, most of the metasurfaces are based on minimum of two layers which have inductive grids on one layer and capacitive structures on the other layer [11] [12]. However, it is possible to design planer surface on one layer that involves a less complicated fabrication process, thus reducing the cost and complexity.

In this paper, we propose a metasurface-based planar lens antenna using a single layer resonant structure at the top of a single patch antenna. The resonant structure is used for focusing, narrowing the beam and as a result, increasing the gain of the single patch antenna without feeding network complexities. At first, a single patch antenna is designed considering probe feeding that can give maximum realized gain (simulated) of 7.2 dBi at 10 GHz. Then a novel single layer metasurface is analysed based on a unit cell of circular patch, integrated with a sub wavelength rectangular slot. Finally, the metasurface is integrated with the single patch at a distance of $\lambda/2$. The metasurface acts as the lens for the antenna and it can increase the realized gain of the antenna from 7.2 dBi to 16.3 dBi. The single antenna and the metasurface are both fabricated. The measured and EM (HFSS) simulated results are compared in terms of reflection coefficient, radiation pattern and max gain of the antenna. It is found that there is a very good agreement (difference in gain $\leq$ 0.4 dB) between the measured and simulated results.

The next section is divided into two subsections. The first subsection gives a brief overview of the results of planar lens antenna based on non-resonant structure. In the second subsection, the importance of resonant planar metasurface and a design methodology using unit-cell simulation results to control the phase magnitude of the metasurface are presented. Moreover, simulation and measured results are compared.

II. Antenna and Metasurface

In this section, the theory and physical dimensions of the metasurface based lens antenna are given. For the source element of the metasurface, a single element antenna based

This work is financed by the Saxon State government out of the State budget approved by the Saxon State Parliament.

DOI 10.1109/EuCNC/6GSummit54941.2022.9815736

on a microstrip patch design is used. The analyses of resonant and non-resonant planar structures are presented.

A. Non-resonant planar lens

This subsection covers the results and discussions related to a non-resonant planar lens antenna. A simple planar lens-based antenna can be designed by placing a superstrate at the top of a single patch antenna as shown in Fig. 1(a). To assure proper functionality of the whole antenna, the superstrate should have a high permittivity value and should be placed at a distance chosen according to the equation 1 which makes the round trip phase feasible for broadside radiation direction ($\theta_p = 0$). Moreover, the thickness of the superstrate should be set according to equation 2. In the above example, a microstrip patch antenna is used as the source which is designed at 10 GHz on a normal RF substrate of Rogers 4350 with a thickness of 0.508 mm. Contrarily, the superstrate needs to satisfy the specific design rules as mentioned before. Thus, its permittivity is chosen high around 20 and the height and thickness of the superstrate are computed to be around 15 mm and 1.677 mm at 10 GHz, respectively. This simple form of the antenna with a superstrate can shape the beam and increase the gain of the antenna up to 18.3 dBi at 10 GHz as shown in Fig 1(b). Nevertheless, realizing such antennas in practice is difficult, given that the requirements of the high permittivity material and its specific thickness requirements have to be met.

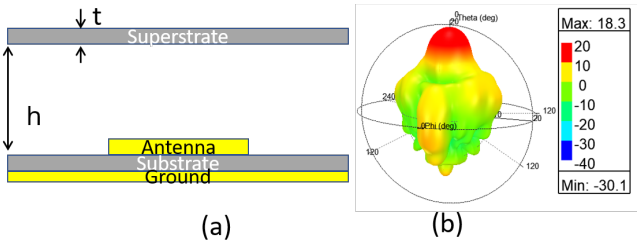

Fig. 1. A simple form of (a) lens based antenna and (b) 3D realized gain pattern

$$h = \frac{\lambda/2}{\sqrt{\epsilon_r - \sin^2\theta_p}} \tag{1}$$

$$t = \frac{\lambda/4}{\sqrt{\epsilon_r - \sin^2\theta_p}} \tag{2}$$

B. Resonant planar lens

The metasurface consists of a 2D array of sub-wavelength unit cells based on circular patch metals, integrated with rectangular slots acting as a planar lens after being placed on the top of the antenna. The metasurface is designed on one side of the same substrate of Rogers 4350 and with the same thickness. The unit cell of the metasurface is shown in Fig 2 and its dimension is around 10.635 mm x 10.635 mm (Uc_x x Uc_y) with a circular patch having a radius of 4.84 mm (Uc_R). The sub-wavelength rectangular slot of 7.65 mm (Uc_L) is etched in the center of the circular patch and its orientation plays a vital role with respect to the polarization of the antenna in order to have proper filtering of the beam pattern and increasing the gain. For ensuring proper performance of the antenna, the slots must be etched perpendicular to the polarization of the antenna.

The unit cell simulation is a paramount part of the meta-surface design and it aids in evaluating as well as extracting the reflection phase and magnitude of the metasurface. The unit cell simulations are performed by using the Floquet ports while considering master and slave boundary conditions of the HFSS as shown in Fig 2. These extracted information helps in deciding the distance between the metasurface and the antenna. Table I shows the optimized values of the unit cell and the overall dimensions of the metasurface. Fig. 3 shows the simulated results of the reflection and transmission coefficients as well as the reflected phase values of the metasurface. The distance between the antenna and metasurface is decided according to equation 3. Where ϕ_m and ϕ_g are the reflected phases from the metasurface and the antenna ground plane, respectively. The estimated phase value from the reflection coefficient of the metasurface requires positioning it according to equation 3 at a distance of approximately $\lambda/2$ (15 mm) from the ground plane in order to ensure having a correct phase in the far-field for constructive interference in the broadside radiation direction. For the fabrication purpose, the metasurface must be large enough to have a certain number of unit cells towards achieving the desired performance after its integration. Fig 4 shows how the gain of the meta-antenna increases with respect to the number of unit cells of the metasurface. Therefore in order to keep the gain of the antenna above 15 dBi, the dimensions of metasurface are chosen to be 86 mm by 86 mm with 8 unit cell by 8 unit cell as shown in Fig 5 (b). The magnitude of the reflection coefficient decides the maximum gain of the antenna according to equation 4 and the calculated directivity of the antenna is around 16.8 dBi.

Fig 5 shows the fabricated single element antenna, metasurface and how the planar lens is integrated on the top of a single patch for the desired performance. Four plastic screws are used at the four corners of the antenna for aligning and fixing a distance of $\lambda/2$ between the antenna and the metasurface as shown in Fig 5

$$h1 + t\sqrt{\epsilon_r} = \frac{(\Phi_m + \phi_g)\lambda}{4\pi} + \frac{N\lambda}{2} \qquad N = 0, \pm1, \pm2, .. \tag{3}$$

$$D = 10\log\frac{1+|\Gamma|}{1-|\Gamma|} \tag{4}$$

Fig 6 shows the effect of the slot rotation on the reflection coefficient of the antenna. The two resonances can be controlled by the rotation of the slot. Furthermore, the antenna bandwidth can be enhanced at the expense of the lower gain and reduced filtering capability of the antenna radiation pattern as shown in Fig 4. Fig 7 shows the measured and simulated results of the meta-antenna. In the absence

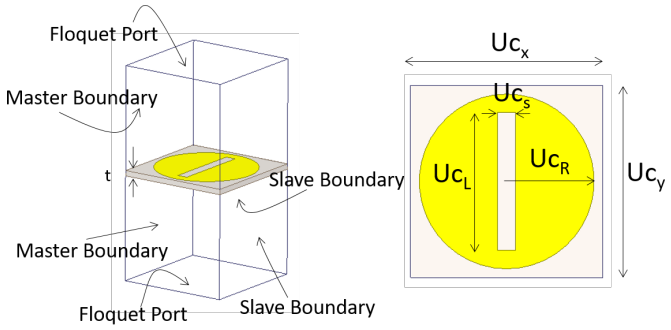

Fig. 2. Unit cell simulation of metasurface with master and slave boundary conditions

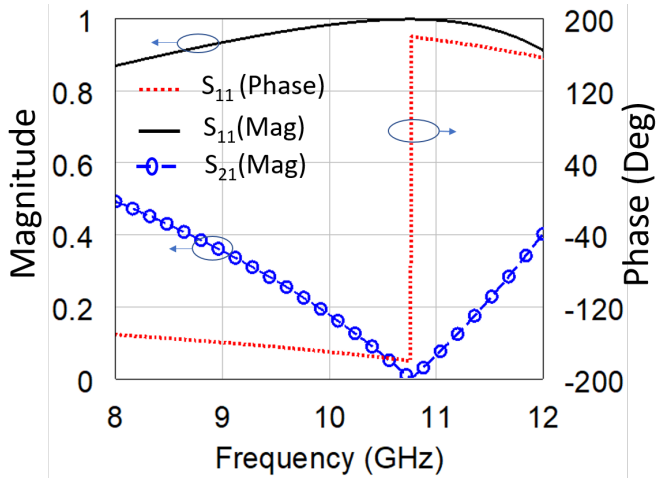

Fig. 3. Magnitude and Phase response of the metasurface lens

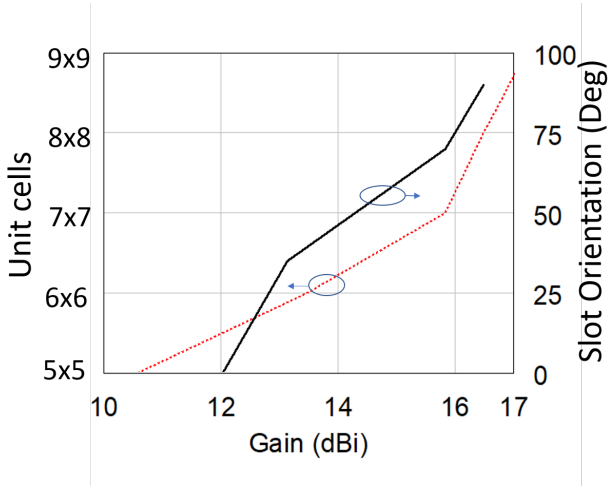

Fig. 4. Gain of the meta-antenna with respect to number of unit cells and rotation of the slot with respect to the antenna

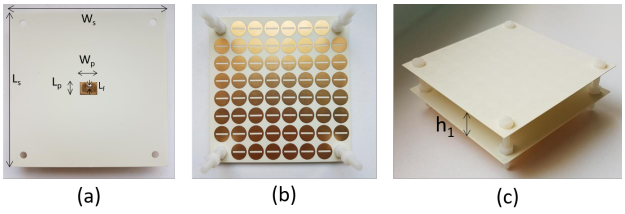

Fig. 5. Fabrication of (a) Antenna (b) Metasurface (c) Integration of metasurface with antenna

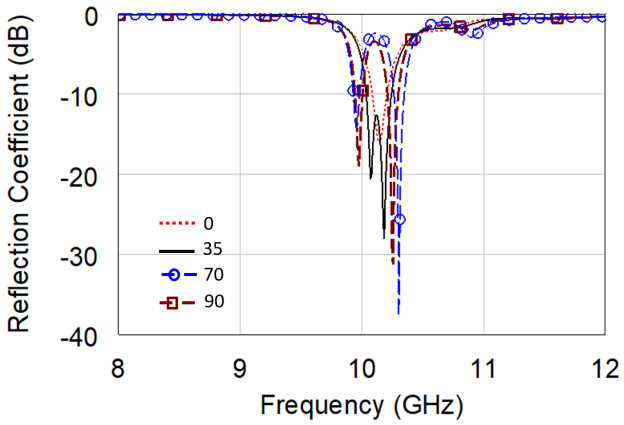

Fig. 6. Analysis of reflection coefficient of the antenna with respect to the orientation of the slot of the metasurface

of the metasurface, the single patch antenna resonates at approximately 10.4 GHz as shown in Fig 7. The inclusion of the planar lens creates a coupling with the antenna and generates two resonances; one at 10 GHz and another at approximately 10.4 GHz. Comparison of the simulation and the measurement results shows a good concord between them as shown in Fig 7. Moreover, the snapshots from the animated current distribution on the metasurface at 10 GHz are shown in Fig 8. The switching between high and low current distribution

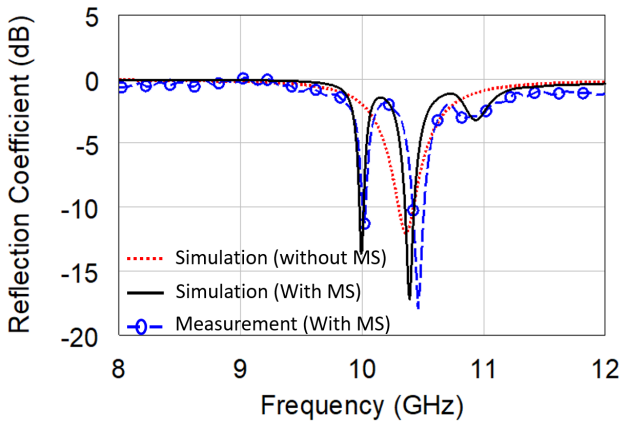

Fig. 7. Reflection coefficient results of the antenna with and without metasurface layer (MS = metasurface)

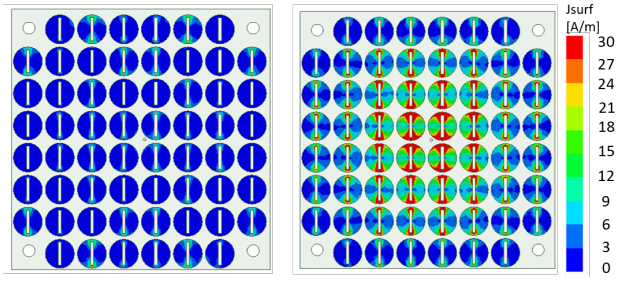

Fig. 8. Snapshots from the animated current distribution plots of the metasurface at 10 GHz

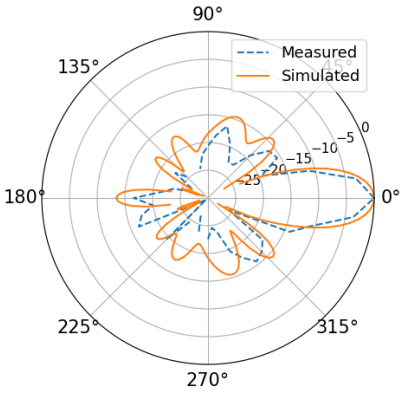

Fig. 9. Measured and simulated 2D radiation pattern of the meta-antenna in the E-Plane at 10 GHz

demonstrates its radiation behavior. In addition, the maximum current distribution at the center unit cells exhibits directive and focusing characteristics of the beam in the far-field.

According to the simulations, the maximum realized gain values of the antenna are estimated to be approximately 16.3 dBi and 13.2 dBi at 10 GHz and 10.4 GHz, respectively. Fig 9 and Fig 10 show the measured and simulated radiation patterns of the meta-antenna in the E-plane and H-plane, respectively. The measured results have a very good agreement

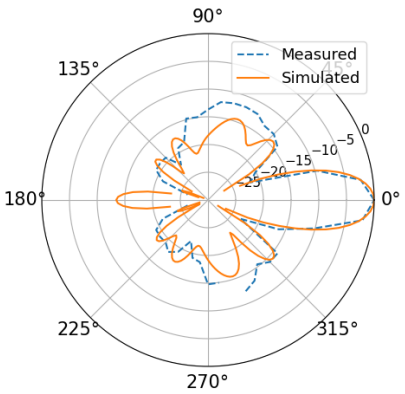

Fig. 10. Measured and simulated 2D radiation pattern of the meta-antenna in the H-Plane at 10 GHz

TABLE I
META-ANTENNA AND UNIT CELL PHYSICAL DIMENSIONS

Parameters	Antenna (mm)	Metasurface (mm)
L_s	86	86
W_s	86	86
L_p	7.1	-
W_p	10	-
L_f	1.2	-
Uc_x	-	10.635
Uc_y	-	10.635
Uc_s	-	0.9
Uc_L	-	7.65
Uc_R	-	4.84
t	0.508	0.508

with EM simulated patterns. The gain of the meta-antenna with a commercial horn antenna with a known gain is estimated around 16 dBi and 12.8 dBi at 10 GHz and 10.4 GHz, respectively, which are very close to the maximum simulated gain values.

Furthermore, this work is compared to other recently published articles. Table II shows the summary of comparison and it is clearly shown that the proposed design is the only design using single layer metasurface. The radiation efficiency of the antenna is also compared and it is found that our design based on one layer has the highest radiation efficiency of more than 90 %. Moreover, the half power beam-width of the antenna is 18° which is beneficial for radar and point to point communication systems

III. CONCLUSIONS

In this work, a metasurface-based single-layer planar lens for shaping beam and increasing the gain of a single element patch antenna has been investigated. The feasibility of increasing the gain with a less complicated fabrication process by combining inductive and capacitive features on a single layer is validated with measurements. Such high gain meta-antennas with single antenna element can play a vital role in simplifying the front end connections of the future sixth generation (6G) integrated systems, enabling low power applications in battery-driven devices. As a forth work, different combinations of meta-unit cells can be used for further reduction of the side lobes. The concept can also be further extended to multiple antennas which can be used for transmission, reception, and beam steering purposes at different frequency bands.

ACKNOWLEDGEMENT

This work is financed by the Saxon State government out of the State budget approved by the Saxon State Parliament. The authors would like to acknowledge the contribution of Tim Hentschel and Gerhard Fettweis to this work.

REFERENCES

[1] C. De Lima *et al.*, "Convergent communication, sensing and localization in 6g systems: An overview of technologies, opportunities and challenges," *IEEE Access*, vol. 9, pp. 26 902–26 925, 2021.

TABLE II
COMPARISON OF THE META-ANTENNA WITH THE LITERATURE REVIEW

References	Antennas	Size (λ_0)	Bandwidth (%)	Max Gain (dBi)	SLL (dB)	HPBW	Radiation Eff. (%)	Layers
[11]	2	1.4 x 1.4 x 0.5	21	15.1	NA	45°	>75	2
[12]	1	4.43 x 4.43 x 0.0625	3.15	15.8	NA	30°	NA	2
[13]	1	1.9 x 1.9 x 0.5	21.5	16.1	NA	NA	30	2
[14]	1	2.88 x 2.88 x 0.66	32.3	14	-18	>30°	NA	4
[15]	1	3.2 x 3.2 x 0.033	1.1	15	<-10	18°	NA	>2
[16]	2x2	1.5 x 1.5 x 0.11	24.3	12.5	<-19.5	NA	53.7	2
[17]	1	1.75 x 1.75 x 0.11	29.3	11.45	NA	>25°	78	2
[18]	1	1.78 x 1.78 x 0.09	3.3+1.9	10.2	-12	38°	NA	2
[19]	2x2	2.8 x 2.8 x 0.5	26.9	15.7	<-10	25°	86.8	2
This Work	1	2.83 x 2.83 x 0.5	0.55+0.78	16	<-13	18°	91.38	1

λ_0 Center frequency wavelength, ^{SLL} Side lobe level, ^{HPBW} Half power beam width,

[2] E. Y. Terán-Bahena, S. C. Sejas-García, and R. Torres-Torres, "Characterization of transmission lines on pcb from s-parameters by determining the dielectric and conductor losses at the crossover frequency," *IEEE Transactions on Components, Packaging and Manufacturing Technology*, vol. 8, no. 5, pp. 867–874, 2018.

[3] S. C. Sejas-Garcia, R. Torres-Torres, and R. S. Murphy-Arteaga, "Modeling transmission lines on silicon in the frequency and time domains from *s*-parameters," *IEEE Transactions on Electron Devices*, vol. 59, no. 6, pp. 1803–1806, 2012.

[4] Y. Dong and T. Itoh, "Metamaterial-based antennas," *Proceedings of the IEEE*, vol. 100, no. 7, pp. 2271–2285, 2012.

[5] X. Yang, Y. Liu, Y.-X. Xu, and S.-x. Gong, "Isolation enhancement in patch antenna array with fractal uc-ebg structure and cross slot," *IEEE Antennas and Wireless Propagation Letters*, vol. 16, pp. 2175–2178, 2017.

[6] Z. L. Ma, C. H. Chan, K. B. Ng, and L. J. Jiang, "A collimated surface-wave-excited high-impedance surface leaky-wave antenna," *IEEE Antennas and Wireless Propagation Letters*, vol. 16, pp. 2082–2085, 2017.

[7] Y. He *et al.*, "Short-length and high-aperture-efficiency horn antenna using low-loss bulk anisotropic metamaterial," *IEEE Antennas and Wireless Propagation Letters*, vol. 14, pp. 1642–1645, 2015.

[8] L.-Y. Liu and B.-Z. Wang, "A broadband and electrically small planar monopole employing metamaterial transmission line," *IEEE Antennas and Wireless Propagation Letters*, vol. 14, pp. 1018–1021, 2015.

[9] D. R. Jackson, P. Burghignoli, G. Lovat, and F. Capolino, "The role of leaky waves in fabry-pérot resonant cavity antennas," in *2014 IEEE-APS Topical Conference on Antennas and Propagation in Wireless Communications (APWC)*, 2014, pp. 786–789.

[10] J. L. Volakis, "Antenna engineering handbook. 4th ed. (chapter 11)," *New York: McGraw-Hill*, 2007.

[11] R. Lian, Z. Tang, and Y. Yin, "Design of a broadband polarization-reconfigurable fabry–perot resonator antenna," *IEEE Antennas and Wireless Propagation Letters*, vol. 17, no. 1, pp. 122–125, 2018.

[12] A. Ghasemi, S. N. Burokur, A. Dhouibi, and A. de Lustrac, "High beam steering in fabry–pérot leaky-wave antennas," *IEEE Antennas and Wireless Propagation Letters*, vol. 12, pp. 261–264, 2013.

[13] A. Lalbakhsh *et al.*, "Single-dielectric wideband partially reflecting surface with variable reflection components for realization of a compact high-gain resonant cavity antenna," *IEEE Transactions on Antennas and Propagation*, vol. 67, no. 3, pp. 1916–1921, 2019.

[14] M. W. Niaz *et al.*, "Wideband fabry–perot resonator antenna employing multilayer partially reflective surface," *IEEE Transactions on Antennas and Propagation*, vol. 69, no. 4, pp. 2404–2409, 2021.

[15] M. M. Honari, P. Mousavi, and K. Sarabandi, "Miniaturized-element frequency selective surface metamaterials: A solution to enhance radiation of rfics," *IEEE Transactions on Antennas and Propagation*, vol. 68, no. 3, pp. 1962–1972, 2020.

[16] S. Jagtap *et al.*, "A wideband microstrip array design using ris and prs layers," *IEEE Antennas and Wireless Propagation Letters*, vol. 17, no. 3, pp. 509–512, 2018.

[17] W. Cao *et al.*, "Wideband circularly polarized fabry–perot resonator antenna in ku-band," *IEEE Antennas and Wireless Propagation Letters*, vol. 18, no. 4, pp. 586–590, 2019.

[18] S. Vaid and A. Mittal, "A low profile dual band resonant cavity antenna," *International Journal of RF and Microwave Computer-Aided Engineering*, vol. 27, no. 2, p. e21065, 2017.

[19] C. Yang, X.-W. Zhu, and P. Liu, "A circularly polarized fabry-perot resonant cavity antenna using frequency selective surface-based partial reflecting surface," *International Journal of RF and Microwave Computer-Aided Engineering*, p. e22735, 2021.